STRUCTURAL BIOLOGY COMMUNICATIONS

ISSN 2053-230X

Crystal structure of the SPRY domain of human SPSB2 in the apo state

Yanhong Luo,[a,b] Kefa Li,[a,b] Jinjin Yang,[a,b] Danting Zhang,[a,b] Yuying Zhou[a,b] and Zhihe Kuang[a,b]*

[a]Department of Cell Biology and Institute of Biomedicine, College of Life Science and Technology, Jinan University, Guangzhou 510632, People's Republic of China, and [b]Guangdong Provincial Key Laboratory of Bioengineering Medicine, Guangzhou 510632, People's Republic of China. *Correspondence e-mail: zhihe.kuang@jnu.edu.cn

Received 10 March 2019
Accepted 2 May 2019

Edited by R. L. Stanfield, The Scripps Research Institute, USA

Keywords: SPRY domain of SPRY domain-containing human SOCS box protein 2; SPSB2; SPRY/B30.2 domain; iNOS; apo structure; His_6 tag.

PDB reference: human SPSB2 in the apo state, 6jkj

Supporting information: this article has supporting information at journals.iucr.org/f

The SPRY domain-containing SOCS box protein 2 (SPSB2) is one of four mammalian SPSB proteins that are characterized by a C-terminal SOCS box and a central SPRY/B30.2 domain. SPSB2 interacts with inducible nitric oxide synthase (iNOS) via the SPRY domain and polyubiquitinates iNOS, resulting in its proteasomal degradation. Inhibitors that can disrupt SPSB2–iNOS interaction and augment NO production may serve as novel anti-infective and anticancer agents. The previously determined murine SPSB2 structure may not reflect the true apo conformation of the iNOS-binding site. Here, the crystal structure of human SPSB2 SPRY domain in the apo state is reported at a resolution of 1.9 Å. Comparison of the apo and ligand-bound structures reveals that the iNOS-binding site is highly preformed and that major conformational changes do not occur upon ligand binding. Moreover, the C-terminal His_6 tag of the recombinant protein binds to a shallow pocket adjacent to the iNOS-binding site on a crystallographically related SPSB2 molecule. These findings may help in structure-based and fragment-based SPSB2 inhibitor design in the future.

1. Introduction

The SPRY domain-containing SOCS (suppressor of cytokine signalling) box protein 2 (SPSB2; also named SSB-2 previously) is one of four mammalian SPSB proteins (SPSB1–SPSB4) that are characterized by a C-terminal SOCS box and a central protein–protein interaction module known as the SPRY/B30.2 domain (D'Cruz, Babon *et al.*, 2013; Perfetto *et al.*, 2013). Previously, Kuang and coworkers found that SPSB2 is a negative regulator of inducible nitric oxide synthase (iNOS) that modulates the lifetime of iNOS and controls cellular nitric oxide (NO) production (Kuang *et al.*, 2010). SPSB2 utilizes the SPRY domain to interact with an N-terminal region of iNOS and uses the SOCS box to recruit an E3 ubiquitin ligase complex, resulting in the polyubiquitination and proteasomal degradation of iNOS (Kuang *et al.*, 2010). Subsequently, it has been shown that SPSB1 and SPSB4 also polyubiquitinate iNOS and regulate the proteasomal degradation of iNOS (Lewis *et al.*, 2011; Matsumoto *et al.*, 2011; Nishiya *et al.*, 2011; Wang, Luo *et al.*, 2018). SPSB2-deficient macrophages showed significantly increased iNOS activity and NO production, and were more active in killing *Leishmania major* parasites; therefore, inhibitors that can disrupt the endogenous SPSB2–iNOS interaction and augment NO production may serve as novel anti-infective and anticancer agents (Kuang *et al.*, 2010). Indeed, since this original discovery, a range of inhibitors aiming to disrupt SPSB2–iNOS interaction have been developed by different groups (Yap *et al.*, 2014, 2016; Leung *et al.*, 2014; Harjani *et al.*, 2016; You *et al.*, 2017; Sadek *et al.*, 2018).

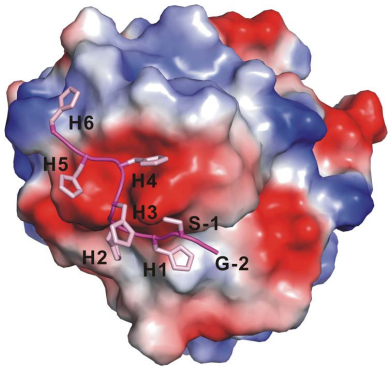

With respect to structural studies, solution (Yao *et al.*, 2005; Masters *et al.*, 2006) and crystal (Kuang *et al.*, 2009) structures of the murine SPSB2 SPRY domain alone, as well as crystal structures of the human SPSB2 SPRY domain in complex with a peptide from the *Drosophila* DEAD-box RNA helicase VASA (Filippakopoulos *et al.*, 2010), with a rationally designed RGD-containing cyclic peptide inhibitor (You *et al.*, 2017) and with cyclic heptapeptides (Sadek *et al.*, 2018) have been reported. Crystal structures have also been reported for GUSTAVUS (a *Drosophila* orthologue of SPSB proteins) in complex with elongins B and C (Woo, Imm *et al.*, 2006) or with a VASA peptide (Woo, Suh *et al.*, 2006). SPRY domains are found in many different proteins, including some tripartite-motif (TRIM) proteins and some RING-finger (RNF) proteins. SPRY domain structures have been determined for TRIM21 (Keeble *et al.*, 2008), TRIM72 (Park *et al.*, 2010), TRIM5α (Biris *et al.*, 2012; Yang *et al.*, 2012), TRIM25 (D'Cruz, Kershaw *et al.*, 2013; Koliopoulos *et al.*, 2018) and TRIM20 (Weinert *et al.*, 2015), and solution NMR has been used to investigate the SPRY domains of TRIM25 (Kong *et al.*, 2015) and RNF135 (Zhang *et al.*, 2019).

It is worth noting that in the crystal structure of ligand-free murine SPSB2 the iNOS-binding site was occupied by residues from crystallographically related molecules (Kuang *et al.*, 2009), raising the question as to whether this structure reflects the true apo conformation of the iNOS-binding site. On the other hand, an apo crystal structure of human SPSB2, without a ligand bound to its iNOS-binding site, has not been determined. Therefore, the extent to which the iNOS-binding site undergoes conformational changes upon binding to iNOS or related inhibitors remains unclear. Here, we report the crystal structure of the human SPSB2 SPRY domain in the apo state at a resolution of 1.9 Å. Comparison of the apo and ligand-bound structures revealed that the iNOS-binding site is highly preformed and that major conformational changes do not occur upon ligand binding. Interestingly, the C-terminal His_6 tag of the recombinant protein binds to a shallow pocket adjacent to the iNOS-binding site on a crystallographically related SPSB2 molecule. These findings may help in structure-based and fragment-based SPSB2 inhibitor design in the future.

2. Materials and methods

2.1. Macromolecule production

Recombinant SPRY domain (residues 22–220) of human SPSB2 (UniProtKB accession No. Q99619) was expressed and purified using a method similar to that described previously (You *et al.*, 2017). Briefly, a cDNA fragment encoding the SPRY domain with a C-terminal His_6 tag was constructed into the pET-15b vector. The recombinant protein was expressed in *Escherichia coli* BL21 (DE3) cells grown in Luria–Bertani medium. The protein was expressed at 18°C for 16 h after induction with 0.1 m*M* isopropyl β-D-1-thiogalactopyranoside when the OD_{600} reached 0.6–0.8. The cells were harvested by centrifugation and were lysed using a cell disruptor (JNBIO).

Table 1
Macromolecule-production information.

Source organism	*Homo sapiens*
DNA source	Synthetic gene
Forward primer	TTTTTTCCATGGGCGACCTCTCCTGTCCC
Reverse primer	TTTTTTCTCGAGTTATCAATGGTGATGATG GTGATGAGAACCCCTTTCGCCCAGGTAG
Cloning vector	pET-15b
Expression vector	pET-15b
Expression host	*E. coli* BL21 (DE3)
Complete amino-acid sequence of the construct produced†	MGDLSCPEGLEELLSAPPPDLGAQRRHGWN PKDCSENIEVKEGGLYFERRPVAQSTDG ARGKRGYSRGLHAWEISWPLEQRGTHAV VGVATALAPLQTDHYAALLGSNSESWGW DIGRGKLYHQSKGPGAPQYPAGTQGEQL EVPERLLVVLDMEEGTLGYAIGGTYLGP AFRGLKGRTLYPAVSAVWGQCQVRIRYL GERGSHHHHHH

† The underlined sequences are the N-terminal cloning artifacts and the C-terminal His_6 tag.

Table 2
Crystallization.

Method	Hanging-drop vapour diffusion
Plate type	24-well plates
Temperature (K)	289
Protein concentration (mg ml^{-1})	4
Buffer composition of protein solution	50 m*M* Tris–HCl pH 7.5, 150 m*M* NaCl, 5 m*M* DTT
Composition of reservoir solution	0.2 *M* ammonium acetate, 0.1 *M* Bis-Tris pH 5.5, 25%(*w*/*v*) polyethylene glycol 3350
Volume and ratio of drop (µl)	1:1
Volume of reservoir (ml)	0.5

The protein was initially purified using an Ni–NTA column (GE Healthcare) and was further purified by gel filtration using a HiLoad 16/600 Superdex 75 column (GE Healthcare) equilibrated against buffer consisting of 50 m*M* Tris–HCl pH 7.5, 150 m*M* NaCl, 5 m*M* DTT. The protein was concentrated using Amicon centrifugal filter units (Merck Millipore). Macromolecule-production information is summarized in Table 1.

2.2. Crystallization

Purified protein samples at concentrations of 4, 6 and 12 mg ml^{-1} were centrifuged at 15 700*g* for 10 min to clarify the solution prior to setting up crystallization trials. Crystallization trials were carried out using the hanging-drop vapour-diffusion method at 16°C. Initial crystallization trials were performed using commercial sparse-matrix screens (PEG/Ion, PEG/Ion 2 and Index from Hampton Research). The crystals used for data collection and structure determination were obtained from a solution consisting of equal volumes (1 µl) of 4 mg ml^{-1} protein solution and reservoir solution consisting of 0.2 *M* ammonium acetate, 0.1 *M* Bis-Tris pH 5.5, 25%(*w*/*v*) polyethylene glycol 3350. Crystallization information is summarized in Table 2.

2.3. Data collection and processing

Prior to data collection, crystals were transferred into a cryoprotectant solution consisting of the reservoir solution

Table 3
Data collection and processing.

Values in parentheses are for the outer shell.

Diffraction source	BL17U, SSRF
Wavelength (Å)	0.9792
Temperature (K)	100
Detector	EIGER 16M
Crystal-to-detector distance (mm)	250
Rotation range per image (°)	1
Total rotation range (°)	360
Exposure time per image (s)	0.2
Space group	$P12_11$
a, b, c (Å)	32.45, 75.10, 79.20
α, β, γ (°)	90, 101.38, 90
Mosaicity (°)	0.3
Resolution range (Å)	34.49–1.90 (1.95–1.90)
Total No. of reflections	96555 (6709)
No. of unique reflections	28566 (2029)
Completeness (%)	97.3 (95.1)
Multiplicity	3.4 (3.3)
$\langle I/\sigma(I)\rangle$	7.6 (2.9)
R_{meas}	0.184 (0.813)
Overall B factor from Wilson plot (Å^2)	13.5

Table 4
Structure solution and refinement.

Values in parentheses are for the outer shell.

PDB code	6jkj
Resolution range (Å)	34.49–1.90 (1.95–1.90)
Completeness (%)	97.1 (94.9)
σ Cutoff	None
No. of reflections, working set	27047 (1920)
No. of reflections, test set	1502 (104)
Final R_{cryst}	0.217 (0.421)
Final R_{free}	0.270 (0.449)
No. of non-H atoms	
Protein	2933
Water	132
Total	3065
R.m.s. deviations	
Bonds (Å)	0.009
Angles (°)	1.555
Average B factors (Å^2)	
Protein	20.98
Water	24.28
Clashscore	4
Ramachandran plot	
Most favoured (%)	97.1
Allowed (%)	2.9
Outliers (%)	0

supplemented with 25%(*v*/*v*) glycerol and were immediately flash-cooled in liquid nitrogen. A 1.9 Å resolution X-ray diffraction data set was collected from a single crystal on beamline BL17U (Wang, Zhang *et al.*, 2018) at the Shanghai Synchrotron Radiation Facility (SSRF), Shanghai, People's Republic of China at a wavelength of 0.9792 Å at 100 K. The data were processed using the *XDS* package (Kabsch, 2010) and the *xia*2 system (Winter, 2010) with the *CCP*4 package (Winn *et al.*, 2011). Scaling was performed with *AIMLESS* (Evans, 2011). Detailed statistics for data collection and processing are shown in Table 3.

2.4. Structure solution and refinement

The structure was determined by molecular replacement with *MOLREP* (Vagin & Teplyakov, 2010) using the crystal structure of SPSB2 in complex with a VASA peptide (PDB entry 3emw; Filippakopoulos *et al.*, 2010). The structural model was built in *Coot* (Emsley & Cowtan, 2004) and refined using *REFMAC*5 (Murshudov *et al.*, 2011). The coordinates have been deposited in the Protein Data Bank with PDB code 6jkj. Structure-solution and refinement statistics are provided in Table 4. Structural figures were prepared using the *PyMOL* molecular-graphics system (Schrödinger).

3. Results and discussion

3.1. Apo structure of the human SPSB2 SPRY domain

The recombinant human SPSB2 SPRY domain contained SPSB2 residues 22–220 plus two cloning-artifact residues (MG) at the N-terminus and two linker residues followed by a His_6 tag (GSHHHHHH) at the C-terminus. The protein crystallized in space group $P12_11$ and the structure was determined at 1.9 Å resolution (PDB entry 6jkj). There are two molecules in the asymmetric unit, with a Matthews coefficient of 2.07 Å^3 Da^{-1} and a solvent content of 40.6% (Matthews, 1968). A total of 195 and 199 of the 209 residues were modelled for chains *A* and *B*, respectively. Because of a lack of continuous density, the four N-terminal residues, the 145–148 region and seven C-terminal residues of chain *A* were not modelled, whereas in chain *B* the six N-terminal residues, the 146–148 region and Gly158 were not modelled. Notably, the C-terminal His_6 tag is disordered in chain *A* but is structured in chain *B* and binds to a crystallographically related molecule (see below). Apart from this there are no significant structural differences between chain *A* and chain *B*; they can be superimposed very well with a root-mean-square deviation (r.m.s.d.) of 0.14 Å for 154 C^α atoms. Overall, the structure exhibits good geometry, with 97.1% of the residues in the most favoured region of the Ramachandran plot, 2.9% in the allowed region and no outliers. Consistent with previously reported crystal structures (Kuang *et al.*, 2009; Filippakopoulos *et al.*, 2010), the SPRY domain of SPSB2 consists of two short helices packed against a bent β-sandwich that is formed by two β-sheets wrapped around a long loop extending from the central strands of the concave β-sheet (Fig. 1). The central region of this loop participates in iNOS binding, and Tyr120 on the tip of the loop is indispensable (Kuang *et al.*, 2010). The opposite side of the domain close to the N-terminal helix is known to form the support for the C-terminal SOCS box (not included in this construct) that interacts with elongins B and C to recruit an ubiquitin ligase complex (Woo, Imm *et al.*, 2006).

The SPRY domains of human and murine SPSB2 share 92% amino-acid sequence identity (data not shown). The apo structure of the human SPSB2 SPRY domain closely matches that of murine SPSB2, with an r.m.s.d. of 0.34 Å for 163 C^α atoms (Fig. 2*a*). Nevertheless, large structural differences are seen in the 153–163 region (upper right in Fig. 2*a*). It has been shown that the corresponding regions in SPRY/B30.2 domains from different proteins have large-amplitude motions in solution and adopt different conformations (Yao *et al.*, 2006). To reveal the possible conformational changes that the iNOS-

binding site undergoes upon ligand binding, the apo structure reported here was superimposed on the structure of the human SPSB2 SPRY domain in complex with a cyclic peptide inhibitor, cR8, which was designed to mimic the bound conformations of iNOS residues (You *et al.*, 2017). The apo and inhibitor-bound structures aligned very well, including the 153–163 region, with an r.m.s.d. of 0.16 Å for 163 C^{α} atoms (Fig. 2*b*). Surprisingly, when the iNOS-binding residues in these three structures were analyzed in detail, we found that the side chains of several key iNOS-binding residues possess different conformations in the human and murine ligand-free structures (Fig. 2*c*). Specifically, the loop residues Ala205–Gln211 adopt different positions and the side chains of Trp207 and Gln209 have different orientations (Fig. 2*c*). On the other hand, the side-chain conformations of iNOS-binding residues are essentially identical in both the apo and inhibitor-bound human structures, including Arg68, Ala72, Thr102, Tyr120, Val206, Trp207 and Gln209 (Fig. 2*d*). Therefore, these results indicate that the iNOS-binding site is highly preformed, at least in the crystals, and major conformational changes do not occur upon ligand binding. Our findings that the human apo structure superimposes better with the human ligand-bound structure than with the murine 'apo' structure were somewhat unexpected, but can be reconciled by the fact that the iNOS-binding site in the murine 'apo' structure was actually occupied by some amide side chains from crystallographically related molecules (Kuang *et al.*, 2009). Thus, we conclude that the apo structure of the human SPSB2 SPRY domain reported here is a better model to represent its apo state.

3.2. Binding of the His_6 tag to the crystallographically related molecule

Interestingly, in the structure reported here the C-terminal His_6 tag (including two preceding linker residues) of chain *B* binds to a crystallographically related SPSB2 molecule (denoted chain *B*′), while in chain *A* this C-terminal tail is disordered (Fig. 3*a*). The C-terminal tail of chain *B* shows continuous main-chain electron density and clear side-chain electron density (Supplementary Fig. S1). When chain *B*′ is superimposed on the SPSB2–cR8 complex structure (You *et al.*, 2017) it is evident that the His_6 tag of chain *B* binds to a region on SPSB2 that is adjacent to the iNOS-binding site occupied by the inhibitor cR8 (Fig. 3*b*). Because this structural information may aid in the structure-based design of SPSB2 inhibitors, we have analyzed the interactions in detail. Hence, the hexahistidine residues are numbered His1–His6 and the two linker residues connecting the SPRY domain and the hexahistidines are numbered Gly−2 and Ser−1 accordingly. The C-terminal His_6 tag of chain *B* forms a short 3_{10}-helix-like structure at Ser−1 to His3 and has an extended conformation at His4 to His6 (Fig. 3*b*). The His_6 tag interacts with SPSB2 residues located in three loops, *i.e.* loop Cys51–Ile57, loop Arg68–Asp76 and Gln116–Asp118 in the aforementioned central long loop (Fig. 3*b*), and occupies a shallow pocket on SPSB2 that is negatively charged with significant shape complementarity (Fig. 3*c*). Since the crystal was obtained using a slightly acidic reservoir solution (pH 5.5), the hexahistidine residues may have been protonated and attracted to this negatively charged pocket. Some hydrogen bonds are formed between the C-terminal His_6 tag and the crystallographically related SPSB2 molecule (Fig. 3*d*). The carbonyl group of Ser−1 forms hydrogen bonds to the side chain of Thr117 and the main-chain N atom of Asp118, while the side chain of Ser−1 forms a hydrogen bond to the side chain of Asp118. The main-chain N atom of His2 forms a hydrogen bond to the side chain of Gln116, whereas the main-chain N atoms of both His3 and His4 form hydrogen bonds to the side chain of Asp118. In addition, the His4 carbonyl group and the side chain of His6 form hydrogen bonds to the side chain of

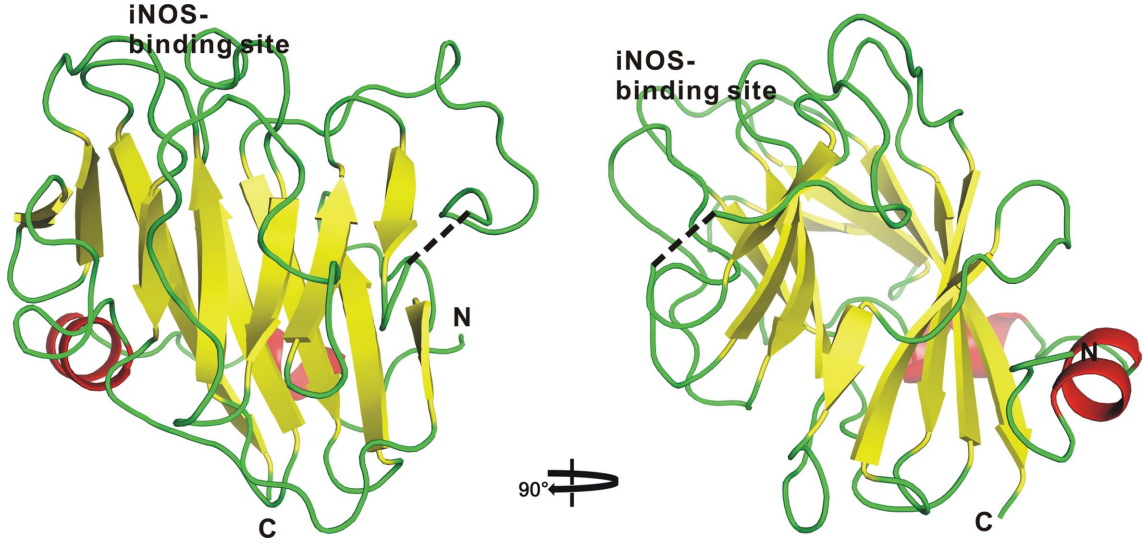

Figure 1
The crystal structure of the human SPSB2 SPRY domain in the apo state. The structure reported here (PDB entry 6jkj, chain *A*) is shown as a cartoon model; α-helices, β-strands and loops are coloured red, yellow and green, respectively. The N- and C-termini and the iNOS-binding site are labelled. The 145–148 region that is missing in the structure is indicated by a black dashed line.

Asn56 and to Pro70, respectively. Nevertheless, the interaction is likely to be weak, firstly because the recombinant protein eluted as a monomer of ∼23 kDa on a gel-filtration column (data not shown) and secondly because only half of the molecules in the crystal are involved in binding the His_6 tag. We then proceeded to use isothermal titration calorimetry (ITC) to measure the binding affinity. An octameric peptide (Ac-GSHHHHHH) was synthesized by Sangon Biotech, Shanghai, People's Republic of China. The purity of the peptide was ∼95% and its observed mass (1026.90 Da) was consistent with its theoretical mass (1026.98 Da) (Supplementary Fig. S2). ITC measurements were carried out in buffers at pH 7.5 and 5.5, both containing 150 m*M* NaCl to mimic the physiological ionic strength. Solutions of 10 µ*M* protein in the cell were titrated by the injection of 500–1000 µ*M* peptide. We found that the binding affinity was too low to be determined under these conditions (Supplementary Fig. S3).

Since inhibitors that can disrupt intracellular SPSB2–iNOS interaction have potential as novel anti-infective and anti-cancer agents (Kuang *et al.*, 2010), some molecules of this type have recently been developed by different groups through structure-based (Yap *et al.*, 2014, 2016; Harjani *et al.*, 2016; You *et al.*, 2017; Sadek *et al.*, 2018) and fragment-based (Leung *et al.*, 2014; Norton *et al.*, 2016) approaches. One strategy to further improve their binding affinities is the linking of the molecule to a compound that can bind to an adjacent binding site on the target protein using a suitable linker (Shuker *et al.*, 1996; Hajduk & Greer, 2007). The novel structure of the His_6 tag bound to a binding pocket adjacent to the iNOS-binding site on human SPSB2 may be therefore of value for developing potent SPSB2 inhibitors in the future.

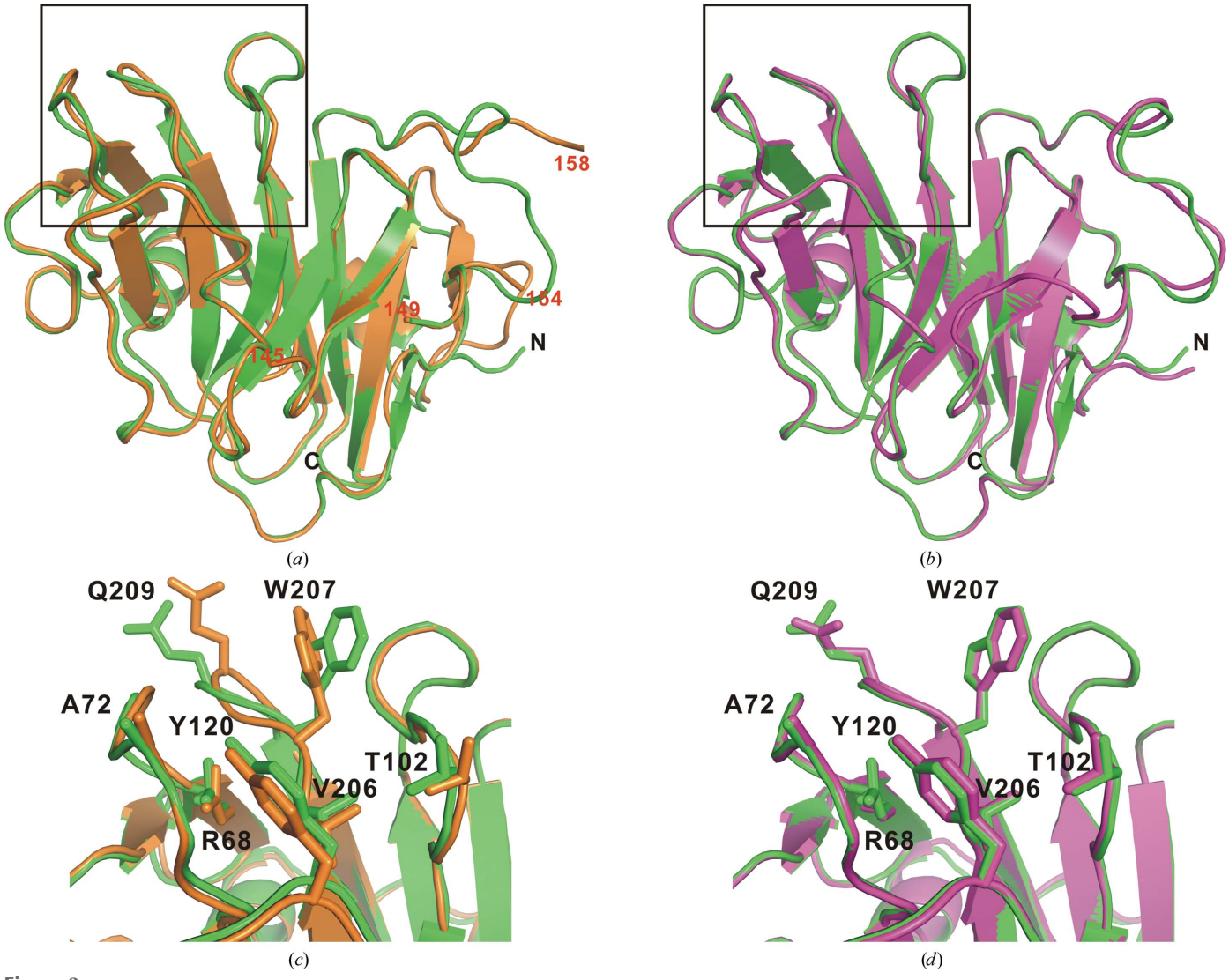

Figure 2
Comparison of apo and ligand-bound structures of the SPSB2 SPRY domain. The apo structure of human SPSB2 reported here (green; PDB entry 6jkj; chain *A*) is superimposed with (*a*, *c*) murine ligand-free SPSB2 (gold; PDB entry 3ek9; Kuang *et al.*, 2009) and (*b*, *d*) human ligand-bound SPSB2 (magenta; PDB entry 5xn3; You *et al.*, 2017). The iNOS-binding site is boxed in (*a*) and (*b*) and is expanded in (*c*) and (*d*), with the side chains that participate in iNOS binding shown and labelled. Murine SPSB2 residues 145, 149, 154 and 158 are labelled in (*a*) to indicate the 146–148 and 155–157 regions that are missing from the structure.

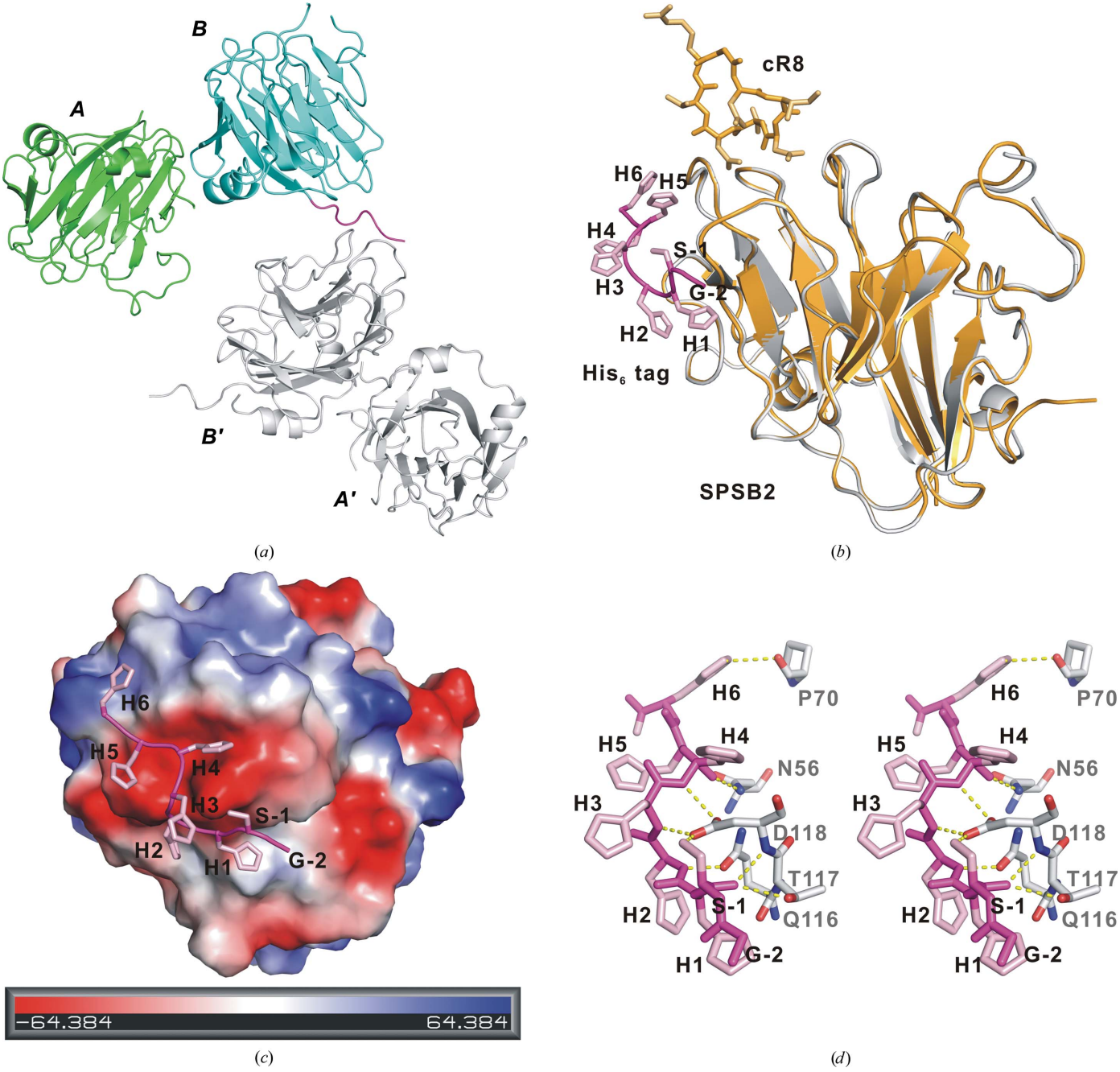

Figure 3
Binding of the C-terminal His_6 tag to the crystallographically related SPSB2 molecule. (*a*) Cartoon representation of the structure (PDB entry 6jkj) showing that the His_6 tag (including two preceding linker residues) of chain *B* binds to the crystallographically related chain *B*′. The His_6 tag of chain *A* is missing from the structure. Chains *A* and *B* are coloured green and cyan, respectively; the His_6 tag of chain *B* is coloured magenta. Chains *A*′ and *B*′ are coloured grey. (*b*) The His_6 tag binds to a region adjacent to the iNOS-binding site. Chain *B*′ (grey) is superimposed with the structure of the SPSB2–cR8 complex (gold; PDB entry 5xn3). The main chain and side chains of the His_6 tag of chain *B* are coloured magenta and light pink, respectively. (*c*) The His_6 tag binds to a shallow pocket on SPSB2. Chain *B*′ is shown as a surface model with electrostatic potentials calculated by *PyMOL*. (*d*) Stereoview of stick models showing hydrogen bonding between the His_6 tag and SPSB2. SPSB2 (chain *B*′) residues are coloured grey; N and O atoms are coloured blue and red, respectively. Hydrogen bonds are indicated by yellow dashed lines.

Acknowledgements

We thank the staff members at both the BL17U and BL19U1 beamlines at the National Facility for Protein Science in Shanghai and the Shanghai Synchrotron Radiation Facility, People's Republic of China and the members of Dr Huihao Zhou's group at Sun Yat-sen University, Guangzhou, People's Republic of China for assistance with diffraction data collection. This work was carried out with the support of Shanghai Synchrotron Radiation Facility (proposals 2017-NFPS-PT-001427 and 2018-NFPS-PT-002086).

Funding information

The following funding is acknowledged: National Natural Science Foundation of China (grant No. 81571539; grant No.

31270817); Fundamental Research Funds for the Central Universities (grant No. 21617443).

References

Biris, N., Yang, Y., Taylor, A. B., Tomashevski, A., Guo, M., Hart, P. J., Diaz-Griffero, F. & Ivanov, D. N. (2012). *Proc. Natl Acad. Sci. USA*, **109**, 13278–13283.

D'Cruz, A. A., Babon, J. J., Norton, R. S., Nicola, N. A. & Nicholson, S. E. (2013). *Protein Sci.* **22**, 1–10.

D'Cruz, A. A., Kershaw, N. J., Chiang, J. J., Wang, M. K., Nicola, N. A., Babon, J. J., Gack, M. U. & Nicholson, S. E. (2013). *Biochem. J.* **456**, 231–240.

Emsley, P. & Cowtan, K. (2004). *Acta Cryst.* D**60**, 2126–2132.

Evans, P. R. (2011). *Acta Cryst.* D**67**, 282–292.

Filippakopoulos, P., Low, A., Sharpe, T. D., Uppenberg, J., Yao, S., Kuang, Z., Savitsky, P., Lewis, R. S., Nicholson, S. E., Norton, R. S. & Bullock, A. N. (2010). *J. Mol. Biol.* **401**, 389–402.

Hajduk, P. J. & Greer, J. (2007). *Nature Rev. Drug Discov.* **6**, 211–219.

Harjani, J. R., Yap, B. K., Leung, E. W. W., Lucke, A., Nicholson, S. E., Scanlon, M. J., Chalmers, D. K., Thompson, P. E., Norton, R. S. & Baell, J. B. (2016). *J. Med. Chem.* **59**, 5799–5809.

Kabsch, W. (2010). *Acta Cryst.* D**66**, 125–132.

Keeble, A. H., Khan, Z., Forster, A. & James, L. C. (2008). *Proc. Natl Acad. Sci. USA*, **105**, 6045–6050.

Koliopoulos, M. G., Lethier, M., van der Veen, A. G., Haubrich, K., Hennig, J., Kowalinski, E., Stevens, R. V., Martin, S. R., Reis e Sousa, C., Cusack, S. & Rittinger, K. (2018). *Nature Commun.* **9**, 1820.

Kong, C., Penumutchu, S. R., Hung, K.-W., Huang, H., Lin, T. & Yu, C. (2015). *Biomol. NMR Assign.* **9**, 313–315.

Kuang, Z., Lewis, R. S., Curtis, J. M., Zhan, Y., Saunders, B. M., Babon, J. J., Kolesnik, T. B., Low, A., Masters, S. L., Willson, T. A., Kedzierski, L., Yao, S., Handman, E., Norton, R. S. & Nicholson, S. E. (2010). *J. Cell Biol.* **190**, 129–141.

Kuang, Z., Yao, S., Xu, Y., Lewis, R. S., Low, A., Masters, S. L., Willson, T. A., Kolesnik, T. B., Nicholson, S. E., Garrett, T. J. & Norton, R. S. (2009). *J. Mol. Biol.* **386**, 662–674.

Leung, E. W. W., Yagi, H., Harjani, J. R., Mulcair, M. D., Scanlon, M. J., Baell, J. B. & Norton, R. S. (2014). *Chem. Biol. Drug Des.* **84**, 616–625.

Lewis, R. S., Kolesnik, T. B., Kuang, Z., D'Cruz, A. A., Blewitt, M. E., Masters, S. L., Low, A., Willson, T., Norton, R. S. & Nicholson, S. E. (2011). *J. Immunol.* **187**, 3798–3805.

Masters, S. L., Yao, S., Willson, T. A., Zhang, J.-G., Palmer, K. R., Smith, B. J., Babon, J. J., Nicola, N. A., Norton, R. S. & Nicholson, S. E. (2006). *Nature Struct. Mol. Biol.* **13**, 77–84.

Matsumoto, K., Nishiya, T., Maekawa, S., Horinouchi, T., Ogasawara, K., Uehara, T. & Miwa, S. (2011). *Biochem. Biophys. Res. Commun.* **409**, 46–51.

Matthews, B. W. (1968). *J. Mol. Biol.* **33**, 491–497.

Murshudov, G. N., Skubák, P., Lebedev, A. A., Pannu, N. S., Steiner, R. A., Nicholls, R. A., Winn, M. D., Long, F. & Vagin, A. A. (2011). *Acta Cryst.* D**67**, 355–367.

Nishiya, T., Matsumoto, K., Maekawa, S., Kajita, E., Horinouchi, T., Fujimuro, M., Ogasawara, K., Uehara, T. & Miwa, S. (2011). *J. Biol. Chem.* **286**, 9009–9019.

Norton, R. S., Leung, E. W. W., Chandrashekaran, I. R. & MacRaild, C. A. (2016). *Molecules*, **21**, 860.

Park, E. Y., Kwon, O.-B., Jeong, B.-C., Yi, J.-S., Lee, C. S., Ko, Y.-G. & Song, H. K. (2010). *Proteins*, **78**, 790–795.

Perfetto, L., Gherardini, P. F., Davey, N. E., Diella, F., Helmer-Citterich, M. & Cesareni, G. (2013). *Trends Biochem. Sci.* **38**, 38–46.

Sadek, M. M., Barlow, N., Leung, E. W. W., Williams-Noonan, B. J., Yap, B. K., Shariff, F. M., Caradoc-Davies, T. T., Nicholson, S. E., Chalmers, D. K., Thompson, P. E., Law, R. H. P. & Norton, R. S. (2018). *ACS Chem. Biol.* **13**, 2930–2938.

Shuker, S. B., Hajduk, P. J., Meadows, R. P. & Fesik, S. W. (1996). *Science*, **274**, 1531–1534.

Vagin, A. & Teplyakov, A. (2010). *Acta Cryst.* D**66**, 22–25.

Wang, T., Luo, S., Qin, H. & Xia, Y. (2018). *Free Radical Biol. Med.* **117**, 90–98.

Wang, Q.-S., Zhang, K.-H., Cui, Y., Wang, Z.-J., Pan, Q.-Y., Liu, K., Sun, B., Zhou, H., Li, M.-J., Xu, Q., Xu, C.-Y., Yu, F. & He, J.-H. (2018). *Nucl. Sci. Tech.* **29**, 68.

Weinert, C., Morger, D., Djekic, A., Grütter, M. G. & Mittl, P. R. (2015). *Sci. Rep.* **5**, 10819.

Winn, M. D., Ballard, C. C., Cowtan, K. D., Dodson, E. J., Emsley, P., Evans, P. R., Keegan, R. M., Krissinel, E. B., Leslie, A. G. W., McCoy, A., McNicholas, S. J., Murshudov, G. N., Pannu, N. S., Potterton, E. A., Powell, H. R., Read, R. J., Vagin, A. & Wilson, K. S. (2011). *Acta Cryst.* D**67**, 235–242.

Winter, G. (2010). *J. Appl. Cryst.* **43**, 186–190.

Woo, J.-S., Imm, J.-H., Min, C.-K., Kim, K.-J., Cha, S.-S. & Oh, B.-H. (2006). *EMBO J.* **25**, 1353–1363.

Woo, J.-S., Suh, H.-Y., Park, S.-Y. & Oh, B.-H. (2006). *Mol. Cell*, **24**, 967–976.

Yang, H., Ji, X., Zhao, G., Ning, J., Zhao, Q., Aiken, C., Gronenborn, A. M., Zhang, P. & Xiong, Y. (2012). *Proc. Natl Acad. Sci. USA*, **109**, 18372–18377.

Yao, S., Liu, M. S., Masters, S. L., Zhang, J.-G., Babon, J. J., Nicola, N. A., Nicholson, S. E. & Norton, R. S. (2006). *Protein Sci.* **15**, 2761–2772.

Yao, S., Masters, S. L., Zhang, J.-G., Palmer, K. R., Babon, J. J., Nicola, N. A., Nicholson, S. E. & Norton, R. S. (2005). *J. Biomol. NMR*, **31**, 69–70.

Yap, B. K., Harjani, J. R., Leung, E. W. W., Nicholson, S. E., Scanlon, M. J., Chalmers, D. K., Thompson, P. E., Baell, J. B. & Norton, R. S. (2016). *FEBS Lett.* **590**, 696–704.

Yap, B. K., Leung, E. W. W., Yagi, H., Galea, C. A., Chhabra, S., Chalmers, D. K., Nicholson, S. E., Thompson, P. E. & Norton, R. S. (2014). *J. Med. Chem.* **57**, 7006–7015.

You, T., Wang, Y., Li, K., Zhang, D., Wei, H., Luo, Y., Li, H., Lu, Y., Su, X. & Kuang, Z. (2017). *Biochem. Biophys. Res. Commun.* **489**, 346–352.

Zhang, D., Wei, H., Xue, H., Guo, S., Wu, B. & Kuang, Z. (2019). *Biomol. NMR Assign.*, https://doi.org/10.1007/s12104-019-09895-w.